Absolute differential cross section measurements for proton-deuteron elastic scattering at 641.3 and 792.7 MeV

E. Gülmez, S. Beedoe, T. Jaroszewicz, A. G. Ling,* and C. A. Whitten, Jr.
University of California, Los Angeles, California 90024

M. W. McNaughton and J. R. Santana
Los Alamos National Laboratory, Los Alamos, New Mexico 87545

D. L. Adams
Rice University, Houston, Texas 77251

V. R. Cupps†
Rutgers University, New Brunswick, New Jersey 08903

A. J. Simon
Texas A&M University, College Station, Texas 77843

M. L. Barlett, K. H. McNaughton, and P. J. Riley
University of Texas, Austin, Texas 78712
(Received 28 January 1991)

The absolute *p-d* elastic-scattering differential cross sections were measured at 641.3 and 792.7 MeV beam energies over a range of c.m. angles from ~35° to ~115° and ~35° to ~140°, respectively. The longitudinally polarized (*L*-type) proton beam produced by the Lamb-shift ion source at LAMPF was used. The beam intensity was measured to high accuracy (~0.1%) by a scintillator-beam particle-counting system designed and developed prior to the experiment. Typical uncertainties in the absolute cross sections were about 2–3 % total, somewhat larger at back angles. The present results were compared with the existing measurements and the controversy about the previous data at 800 MeV was resolved. The present data can be fit with a relativistic multiple-scattering theory which uses off-mass-shell extrapolations of the nucleon-nucleon amplitudes suggested by the structure of derivative meson-nucleon couplings. Relativistic-impulse-approximation calculations do not fit these data at either energy.

I. INTRODUCTION

Important tests of nucleon-nucleus scattering models are provided by *p-d* elastic scattering. The deuteron is the simplest composite nuclear system available and the relatively complex $\frac{1}{2}-1$ spin structure of the *p-d* system provides a large number of experimental observables to be fit by various models of the scattering process. Among these experimental observables, the unpolarized differential cross section plays an essential role in determining the overall scale of the scattering amplitudes, because bilinear combinations of the scattering amplitudes can be expressed in terms of a spin observable times the unpolarized differential cross section.[1] Hence it is clear that the accuracy of the differential cross section data directly affects the final results of the amplitude calculations.

There are several recent unpolarized cross section measurements at intermediate energies, especially between 300 and 800 MeV. Alder *et al.*[2] measured the unpolarized elastic-scattering cross sections at 316, 364, 470, and 590 MeV with reasonable accuracy (3–4 %), covering mostly backward scattering angles. Booth *et al.*,[3] Boschitz *et al.*,[4] and Albrow *et al.*[5] measured the unpolarized elastic-scattering cross sections at 425, 582, and 594 MeV, respectively, covering a range of angles from 30° to 160°–180° in c.m. (a little less in the case of 594 MeV). The typical uncertainties were 10% or higher. There are unpublished relative elastic-scattering cross section data[6] at 650 MeV mostly covering the forward-scattering angle region. Similarly a small-angle cross section data set was reported by Irom *et al.*[7] at 796 MeV with 4–5 % uncertainty. Unfortunately, the existing differential cross section data covering a broader angular range at 800 MeV (Ref. 8) have large uncertainties (~10%) and the data reported were internally inconsistent. It is easy to show that the conversion from the laboratory reference frame to the c.m. reference frame was done by using the inverse Jacobian. However, the center-of-mass frame values reported in the paper seem to be more consistent with the unpolarized elastic-scattering cross sections at nearby energies. This inconsistency casts doubts on the whole data set and therefore it was necessary to remeasure the unpolarized differential cross sections at 800 MeV with a

higher accuracy. Furthermore, it is also important to know the unpolarized cross sections at 800 MeV to as high a precision as possible, since most of the extant spin observable data[7–15] for the *p-d* elastic scattering has been measured at 800 MeV.

Previously, an experiment was set up to measure the absolute *p-p* elastic-scattering differential cross sections at energies between 500 and 800 MeV with a total uncertainty of $\sim 1\%$.[16] The data presented here were taken using the same setup at 647 and 798 MeV beam energies.[17]

II. EXPERIMENTAL METHOD

The *p-d* elastic-scattering cross section data were taken at the Los Alamos Clinton P. Anderson Meson Physics Facility (LAMPF), EPB (External Proton Beam) area. The nominal beam energies were 647±0.5 and 798±0.5 MeV. The beam energies were measured by using the High Resolution Spectrometer (HRS). The effective beam energies at the center of the liquid-deuterium target were 641.3±0.5 and 792.7±0.5 MeV after taking into consideration the energy loss in the target, vacuum windows, beam counting scintillators, and short sections of air. The total energy loss of the beam in the target was 8.4 and 7.8 MeV for 647 and 798 MeV beams. In fact, the cross sections reported here could be viewed as the average cross sections over an energy range of [637.0, 645.4] and [788.8, 796.6] for 647 and 798 MeV beam energies, respectively.

Throughout the experiment the polarized $P-$ beam was produced by the Lamb-shift ion source. The polarization of the beam was always along the momentum vector of the proton (L type in the Ann Arbor convention[18]) to give the same effect as an unpolarized beam in our detectors. Furthermore, the direction of the polarization vector was reversed every two minutes to cancel out any residual polarization effects. To eliminate dispersion of the beam by the bending magnet, the zero-degree line at the EPB area was chosen. The beam spot size at the target was about 1 mm in diameter at FWHM. The correct orientation of the average beam polarization was obtained and maintained throughout the experiment by the use of a spin precessor upstream of the target. The spin precessor consists of a solenoid and bending magnets which could be set up to precess the beam polarization to the longitudinal direction (L type). The combination of bending magnets also cleans up any impurities in the beam because the magnet parameters were set up for protons at the selected beam energy with very small deviations and the H^- beam is required to change to H^+ at a thin stripper between the first and second magnets.

The beam intensity measurements used a scintillator telescope consisting of three scintillators placed upstream of the target (Fig. 1). A coincidence from at least two of the scintillators was required to accept a particular beam micropulse as being occupied by one or more beam particles. Corrections for multiple occupancies were made by using time-sequenced coincidences of the beam-micropulse-full signal and Poisson statistics. References 19, 20, and 21 give detailed descriptions of the beam

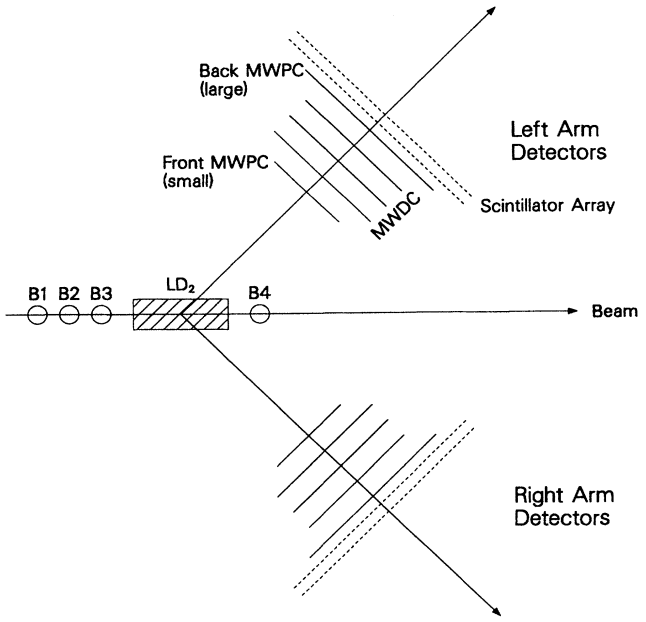

FIG. 1. Experimental setup for measuring the *p-d* elastic-scattering cross sections at 647 and 798 MeV nominal beam energies. The zero-degree beam line at the LAMPF EP-NORTH experimental area was used.

counting setup designed and developed for the absolute cross section measurements and also discuss the performance and limitations of this setup. The average Poisson parameter (beam intensity) for this measurement was about 0.1–0.15 or lower which means that the systematic uncertainty in the beam intensity was around 0.1% because of the beam-particle-counting method used here.[20] An average Poisson parameter of 1.0 means that there is an average number of one particle per beam micropulse. All the data were taken with the 100-ns beam microstructure with an exception of a few runs taken with the 5-ns beam microstructure.

The attenuation of the proton beam was significant enough to merit additional study. A fourth scintillator (5 mm thick and one-third larger in diameter than the main beam-counting scintillators to compensate for small-angle multiple scatterings) placed downstream of the target was used to measure the beam attenuation in the target. The total beam attenuation was obtained by simply comparing the number of coincidences in the upstream beam-counting scintillators with the number of coincidences in all the beam-counting scintillators, upstream and downstream. The measured values for the beam attenuation were 0.926±0.001 and 0.919±0.001 at the 647 and 798 MeV beam energies, respectively. The attenuation measured by the fourth scintillator was also estimated by taking into account the multiple scattering and the total $p+d$ scattering value at these beam energies. The contributions to the multiple scattering from the target assembly and the vacuum windows were determined by measuring the beam attenuation when the target was empty of liquid deuterium and also when the target as-

sembly is moved completely out of the beam. These estimates were 0.926±0.003 and 0.916±0.003 at the 647 and 798 MeV beam energies, respectively. The correction factor for the beam absorption is the average absorption at the middle of the target. The correction factors used for the 647 and 798 MeV proton beams were 0.961 and 0.955, respectively. These correction factors included compensations for beam protons undergoing both small-angle scattering and a legitimate elastic scattering into the detector system.

Liquid deuterium at 23.2 K and 0.09 MPa was used as the target. The target container consisted of a 197-mm-long, 54-mm-diameter cylinder made of 0.125-mm-thick Mylar with 0.075-mm-thick Mylar end caps. There was a cylinder of small diameter (43 mm) inside this container to deflect bubbles from the beam-target interaction region. The local pressure variations in the target flask were eliminated by several holes at the top. This target flask and the accompanying plumbing were placed inside a larger flask (135 mm in diameter and 360 mm long) made of the same material and full of cold deuterium gas. The entire assembly was wrapped with 20 layers of thin (0.006 mm) Mylar and was placed inside an insulating vacuum. The vacuum windows were made of 0.25-mm-thick plain Mylar. The temperature and the pressure of the target were monitored at several different places in the flask. From these temperature and pressure measurements, the exact target temperature, which was used to obtain the correct density of the liquid, was determined accurately. The correct temperature of the target was also used to calculate the thermal contraction (−1.2 mm) of the target flask. In addition to the thermal contraction, the room-temperature measurement of the target flask length (197.7±0.2 mm) was also corrected for the bulging (+0.7 mm total for both ends) of the end caps due to the liquid pressure, to give a corrected length of 197.2±0.2 mm. The length of the target was also obtained by emptying the target and measuring the distance between the two peak positions in the traceback histograms of the particle trajectories to the target position caused by the *p-p* quasielastic scattering in the end caps. This was also corrected for the bowing in the end caps for the full target to give 198.6±0.2 mm. There was no need to correct for the thermal contraction because the empty-target data were taken at ~1 K above the usual running conditions (23.2 K). The final value used in the cross section calculations was the average of these two values and the difference between them was added to the uncertainties in the target length measurements discussed above. Hence the final value used in the cross section calculations was 197.9±0.8 mm. Using the density (0.164 g/cm^3) of the liquid deuterium corrected for the temperature and pressure effects, the target thickness was calculated to be 9.723×10^{-7} particles/μb.

The main experimental setup consisted of two almost identical detector arms (Fig. 1). Each arm had two independent chamber systems: two multiwire proportional chambers (MWPC),[22] three multiwire delay-line-drift chambers (MWDLDC), and vertical and horizontal scintillator planes. The dimensions of the active area of the MWDLDCs were 60 cm×60 cm. The three MWDLDCs were between the two MWPCs. The front and back MWPCs had dimensions of 51 cm×40 cm with 2.00 mm wire spacing and 77 cm×63 cm with 3.01 mm wire spacing, respectively. The vertical (front) scintillator plane consisted of three 4.8-mm-thick scintillators. The horizontal (back) scintillator plane has four 6.4-mm-thick scintillators. The master trigger for the data-acquisition system was formed by a coincidence of at least three scintillator planes. This arrangement made it possible to measure and monitor the individual scintillator plane efficiencies. Typical plane efficiencies were around 99.9%. The overall scintillator efficiency affecting the master trigger was calculated assuming that there is no correlation between planes. For all the regular data-taking runs, the overall efficiency calculated this way was 100% for all practical purposes. These detector arms were placed as close to the target as physically possible to optimize the solid angle covered. The distances between the target center and the detector arm center (roughly the position of the middle MWDLDC) varied between 55 and 102 cm depending on the scattering angle region to be covered. Typical angular ranges subtended by these detector arms (the region illuminated by the whole target and not just a portion of it) were around 25°–35° in polar and 24°–36° in azimuthal angles.

The efficiencies of the individual chambers and the chamber system as a whole were measured by using one set of chambers to monitor the other. First the events that had valid trajectories through one chamber system were determined. Then using these valid events with similar criteria for a valid trajectory, the other set of chambers were tested. The valid events in the first chamber system that could not pass the similar tests in the second system determined the inefficiency of the second system of the chambers. A valid event is defined as an event that has well defined trajectories in both arms that can be traced back to a point in the target (either a *p-p* quasielastic or a *p-d* elastic-scattering event). Since the MWPCs had significantly higher efficiencies compared to the MWDLDCs (~97% as compared to 50% or lower), the MWPCs were used to obtain the scattering yield and the MWDLDCs were used to measure the efficiency of the MWPCs. Typical overall MWPC efficiencies (combination of four MWPCs) were around 97%. Most of the inefficiencies were caused by a few dead wires in the chambers (about 1%) and the delta rays (secondary electrons produced by the passage of charged particles through the chambers).

The data-acquisition live time was monitored throughout the experiment using several different combinations of the coincidence signals of the beam counters and the scintillator planes in the detector arms. Within their uncertainties these were all in agreement. The live time used to correct the final scattering yields was obtained by using the coincidence of the four scintillator planes corrected for the random coincidences and these signals gated with the busy signal. Typical live times were about 80–90 %.

Systematic studies of the live time, the chamber efficiencies, and the beam intensity measurement procedure were made over a wide range of beam intensities

from a Poisson parameter of 0.01 to 2.2 (1.3 fA to 0.28 pA for the 100-ns beam microstructure case with an 8% duty factor). The effects of the different beam intensities on the beam-counting procedure were discussed in Refs. 20 and 21. To keep the live times and the efficiencies high, the Poisson parameter was limited to ≤ 0.2, thereby reducing the systematic uncertainties in these quantities to a negligible amount ($<0.1\%$).

III. ANALYSIS

A VAX750 computer with a CAMAC system was used in data acquisition during the experiment. The CAMAC system was augmented with a MWPC read-out and encoding system.[22] In addition to the *p-d* elastic-scattering events, the *p-p* quasielastic events, which made up 90% of the data recorded, were also taped. These quasielastic events were eliminated during replay by using the following tests.

$\Delta\theta$: the relationships between the kinematical quantities of the scattered and recoiled particles can be easily calculated given the beam and the target kinematical quantities (Fig. 2) as follows:

$$\tan\theta_p = \frac{2(T_B+m_p+m_d)m_d\tan\theta_d}{m_p^2-m_d^2+(T_B+m_p+m_d)^2\tan^2\theta_d} , \quad (1)$$

where T_B is the beam energy, m_p,θ_p,m_d, and θ_d are the mass and the scattering angle of the proton and deuteron, respectively. A similar relationship for *p-p* elastic scattering could be obtained by setting $m_d=m_p$. *p-p* quasielastic scattering has the same kinematic properties as *p-p* elastic scattering except that it has a broad distribution centered around the elastic-scattering curve (Fig. 2 inset). Using the measured recoil angle for the deuteron, the proton-scattering angle can be calculated through the *p-d* elastic-scattering kinematics [Eq. (1)] or vice versa. Then this calculated scattering angle can be compared with the measured scattering angle. A histogram of the difference ($\Delta\theta$) of the calculated and the measured angles for *p-d* elastic scattering was set up and the events outside the main peak centered at zero were rejected [Fig. 3(a)]. This was done for both cases, that is, proton scattered to the left and to the right. The peak centered at zero had a FWHM of $<1°$ caused largely by multiple Coulomb scattering in the target with a smaller contribution from the MWPC resolution.

Energy Loss: another useful test to differentiate between the *p-p* quasielastic and *p-d* elastic-scattering events is the energy loss of the particles detected in the scintillator planes. Energy loss was calculated by taking the geometric average of the pulse heights from the two ends of a scintillator. Broad peaks for protons and deuterons were observed in the energy-loss histograms [Fig. 4(a)]. The events that fall above a certain channel (roughly the peak position for *p-p* quasielastic-scattering events) in at least one of the energy-loss histograms that belonged to the arm in which the deuteron was expected to be detected were accepted as *p-d* elastic events. The gates on these energy-loss histograms were arranged so that good *p-d* elastic-scattering events would not be rejected because of the broadness of the deuteron energy-loss distribution. Hence, this was a loose test.

Time of Flight: the time of flight of the particles detected in one arm relative to the particles detected in the other arm was measured for each event. The offsets for the time-of-flight (TOF) histograms were selected so that the TOF peak for the *p-p* quasielastic-scattering events were centered around zero and the TOF peaks for the *p-d* elastic-scattering events were on the right or left of the *p-p* quasielastic scattering events depending on whether the proton scattered right or left [Fig. 4(b)]. In selecting a good *p-d* elastic scattering event, at least two pairs, out

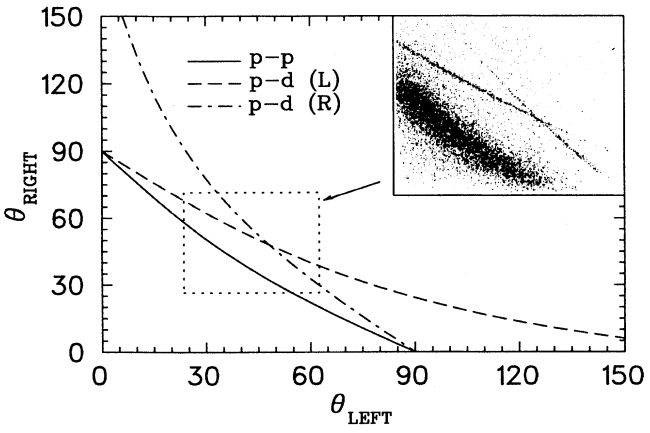

FIG. 2. Kinematics of *p-p* and *p-d* elastic scattering at 800 MeV beam energy. The experimental data displayed by the inset correspond to the area enclosed by the dashed lines.

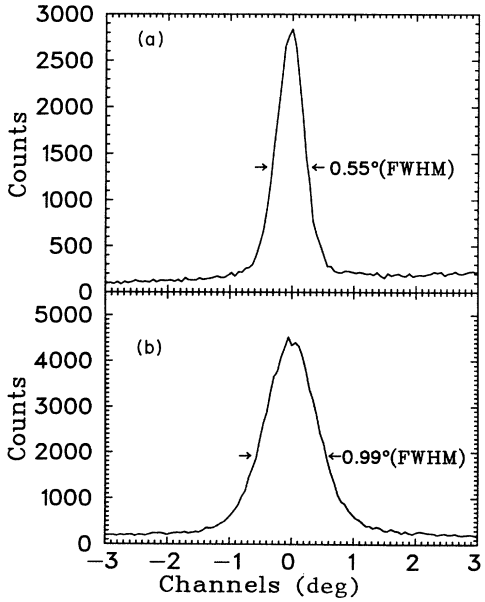

FIG. 3. Typical histograms of the (a) $\Delta\theta$ and (b) $\phi_p+\phi_d$ quantities (explained in the text) for 798 MeV and a 52°–41° angle setting (nominal left and right detector arm settings).

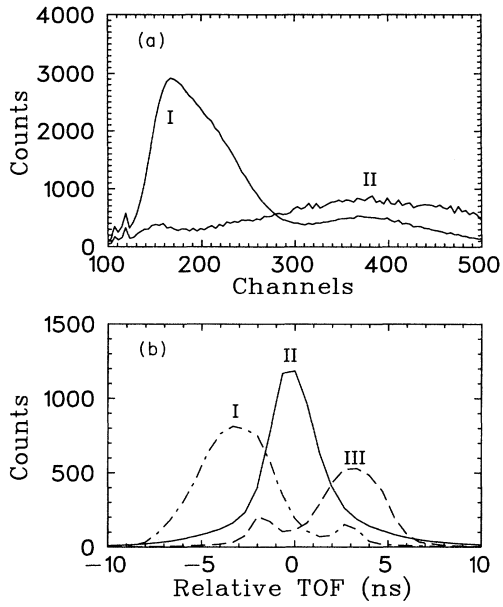

FIG. 4. (a) Typical energy-loss histogram (for front-left scintillator plane) indicating the distribution for protons and deuterons. Curve I corresponds to all the events detected, the *p-p* quasielastic- and *p-d* elastic-scattering events, scaled down by a factor of 10. Curve II represents the events that passed all the required tests except the energy-loss test. (b) An example (between left-front and right-back scintillator planes) of a relative TOF histogram displaying the different types of scattering events: *p-p* quasielastic (curve II) and *p-d* elastic scattering to the right (curve III) and left (curve I). These histograms are from the same settings as Fig. 3. Curve II is scaled down by a factor of 50.

of a possible four pairs of scintillator planes, were required to have the right relative TOF value. Requiring at least three pairs would mean that all four planes of scintillators had a valid event, introducing a four-plane efficiency into the analysis. The master trigger requires at least three planes to have a valid event.

Coplanarity, $\phi_p + \phi_d$, of the scattered and recoiled particles [Fig. 3(b)] and trajectories tracking to the target position were additional tests used in selecting good *p-d* elastic-scattering events.

After determining the good *p-d* elastic-scattering events, several two-dimensional histograms were set up. These were histograms of event distributions as a function of (θ,z),(ϕ,z), and (θ,ϕ), where θ,ϕ, and z were the polar and azimuthal scattering angles and the target position where the scattering occurred, respectively. The correct acceptance of the detector arms was determined as the intersection region of these three different distributions of the good *p-d* elastic-scattering events. The target position z was included to ensure that the acceptance was illuminated by the whole target length. Yields were summed over the ϕ acceptance, within 30- or 50-mr-wide θ bins (placed on proton-scattering angles). An upper limit on the solid-angle uncertainty due to wire chamber resolution and multiple Coulomb scattering is estimated to be 0.5%.

The yields obtained for each bin were also corrected for the absorption of both the scattered particles (including the effects of deuteron breakup) using total cross sections for $d+d$ and $p+d$ scatterings in the target. The correction factors did not include the absorption of the scattered particles outside the target (chambers, air, etc.) which was assumed to be negligible. Typical corrections for the absorption of the scattered and recoiled particles were 3–6 % depending on the scattering angle. The correction for the beam absorption was discussed in Sec. II.

The corrections to the yields for the inefficiences of the chambers, scintillators, and beam counters were minimal. As mentioned above, the scintillator planes and the beam counters were practically 100% efficient. Typical corrections for the chamber inefficiencies were around 3%.

Even though the tests used in the selection of the *p-d* elastic-scattering events were very powerful, there were still some *p-p* quasielastic events resulting in a background that in some cases (forward angles) was as large as ~40%. To subtract the *p-p* quasielastic background from the total yield, two-dimensional histograms were accumulated giving the distribution of the background as a function of θ and ϕ. The events accumulated were the events that passed all the tests that were required for a good *p-d* elastic-scattering event but with a modified $\Delta\theta$ test. The modified $\Delta\theta$ test was set up by placing a gate, half the size of the gate for the $\Delta\theta$ test in selecting a good *p-d* elastic-scattering event, on each side of the main peak, instead of a gate on the main peak itself. Then the background subtraction was achieved by placing the same bins on the two-dimensional background histograms as on the total yield histograms and simply taking the difference as the final scattering yield for a particular bin. The statistical uncertainties reported in Tables I and II include the statistical uncertainties due to the total and background events, in addition to the statistical uncertainties in the efficiency measurements. However, the method outlined here assumes that the background is linear. Further corrections for a higher-order background were included in the final results. These corrections were 0–6 %±0.5–1.5 % depending on the proton-scattering angle.

IV. RESULTS AND CONCLUSIONS

The unpolarized differential cross section data at 641.3 MeV beam energy were taken over a range of proton-scattering angles from 20° to 80° in the laboratory frame of reference [35° to 115° in c.m. or $0.20 < -t < 1.58$ $(\mathrm{GeV}/c)^2$] at three different angular settings of the detector arms [Figs. 5,6,7(a) and Table I]. At more forward-scattering angles, the recoiled deuterons did not have enough energy to penetrate to at least the front scintillator plane because of the energy loss in the target. Hence the forward acceptance of the detectors was limited to 20°. Measurements at more backward angles were not possible because of the available beam time at this energy.

TABLE I. *p-d* elastic-scattering cross sections at 641.3 MeV.

Laboratory angle (deg)	$d\sigma/d\Omega_{lab}$ (μb/sr) [a]	c.m. angle (deg)	$d\sigma/d\Omega_{c.m.}$ (μb/sr) [b]	$-t$ (GeV/c)^2	$d\sigma/dt$ [μb/(GeV/c)^2] [b]
20.63	1589.42±21.30±19.61	34.89	593.34±10.81	0.20	3387.71±61.71
22.92	859.41±16.03±13.23	38.66	327.61±7.93	0.24	1870.48±45.25
25.21	444.88±11.94±9.17	42.39	173.52±5.87	0.29	900.72±33.53
27.50	265.75±6.12±4.82	46.08	106.26±3.11	0.34	606.71±17.78
29.79	200.20±4.82±3.77	49.74	82.22±2.51	0.39	469.45±14.35
32.09	174.93±3.94±3.12	53.35	73.93±2.12	0.44	422.10±12.12
34.38	161.40±2.58±2.23	56.91	70.31±1.48	0.50	401.45±8.47
36.67	152.02±2.25±1.81	60.44	68.39±1.30	0.56	390.46±7.42
38.96	136.47±2.49±1.86	63.91	63.50±1.45	0.62	362.54±8.26
41.54	123.37±1.61±1.36	67.76	59.74±1.02	0.68	341.07±5.83
44.40	105.19±1.45±1.20	71.96	53.37±0.95	0.76	304.69±5.44
47.27	88.48±1.30±0.63	76.07	47.13±0.77	0.84	269.11±4.40
50.13	71.27±1.15±0.52	80.09	39.95±0.71	0.91	228.10±4.05
53.00	56.89±1.00±0.42	84.03	33.63±0.64	0.99	191.99±3.65
55.86	44.60±1.07±0.36	87.88	27.85±0.71	1.06	159.01±4.03
58.73	35.96±1.02±0.31	91.63	23.76±0.71	1.13	135.68±4.04
61.59	29.40±0.92±0.27	95.29	20.60±0.67	1.20	117.64±3.83
64.46	25.86±0.85±0.24	98.85	19.24±0.66	1.27	109.88±3.77
67.32	20.44±0.79±0.21	102.32	16.17±0.65	1.34	92.32±3.70
70.19	18.24±1.09±0.25	105.69	15.37±0.94	1.40	87.77±5.38
73.05	16.32±1.04±0.23	108.97	14.66±0.96	1.46	83.70±5.46
75.92	15.00±1.01±0.52	112.14	14.38±1.09	1.52	82.11±6.20
78.78	13.92±0.95±0.49	115.22	14.26±1.09	1.57	81.44±6.23

[a]Statistical and systematical uncertainties are given separately. The first quantity after the cross section value in this column is the statistical uncertainty and the second one is the systematical uncertainty.
[b]Uncertainties listed in this column are the total uncertainties, that is, the combination of statistical and systematical uncertainties.

TABLE II. *p-d* elastic-scattering cross sections at 792.7 MeV.

Laboratory angle (deg)	$d\sigma/d\Omega_{lab}$ (μb/sr) [a]	c.m. angle (deg)	$d\sigma/d\Omega_{c.m.}$ (μb/sr) [b]	$-t$ (GeV/c)^2	$d\sigma/dt$ [μb/(GeV/c)^2] [b]
19.77	932.36±12.21±11.34	34.33	330.50±5.91	0.24	1519.22±27.15
21.49	551.98±9.26±7.87	37.23	198.91±4.38	0.28	914.35±20.13
23.20	353.06±7.02±5.70	40.10	129.50±3.32	0.32	595.29±15.25
24.92	251.43±2.88±2.84	42.96	93.99±1.51	0.37	432.04±6.96
26.64	229.96±2.48±2.52	45.79	87.71±1.35	0.41	403.17±6.21
28.36	213.48±3.07±2.75	48.60	83.17±1.60	0.46	382.32±7.37
30.08	200.50±2.02±2.13	51.38	79.88±1.17	0.51	367.20±5.37
31.80	189.48±1.86±1.99	54.13	77.29±1.11	0.57	355.26±5.11
33.52	173.27±1.71±1.83	56.86	72.43±1.05	0.62	332.93±4.81
35.24	146.27±1.34±1.38	59.56	62.72±0.83	0.67	288.33±3.80
36.96	130.60±1.23±1.25	62.22	57.51±0.77	0.73	264.35±3.55
38.67	114.00±1.08±1.09	64.86	51.60±0.760	0.79	237.18±3.20
40.39	98.12±1.09±1.00	67.47	45.69±0.69	0.84	210.04±3.17
42.11	83.27±0.80±0.80	70.04	39.93±0.54	0.90	183.55±2.49
44.40	66.35±0.55±0.61	73.42	33.13±0.41	0.98	152.27±1.88
47.27	50.97±0.51±0.35	77.56	26.82±0.32	1.07	123.30±1.49
50.13	36.52±0.44±0.25	81.61	20.30±0.28	1.17	93.31±1.31
53.00	28.25±0.38±0.20	85.56	16.62±0.25	1.26	76.39±1.17
55.86	21.02±0.35±0.15	89.41	13.11±0.24	1.35	60.25±1.10
58.73	16.66±0.31±0.13	93.16	11.04±0.22	1.44	50.74±1.03
61.59	12.85±0.31±0.10	96.82	9.05±0.23	1.53	41.61±1.05
64.46	10.91±0.28±0.09	100.37	8.19±0.22	1.61	37.67±1.03
67.32	8.92±0.26±0.08	103.82	7.14±0.21	1.69	32.82±0.98
70.19	7.41±0.28±0.07	107.16	6.34±0.25	1.77	29.13±1.13

TABLE II. (*Continued*).

Laboratory angle (deg)	$d\sigma/d\Omega_{lab}$ (μb/sr) [a]	c.m. angle (deg)	$d\sigma/d\Omega_{c.m.}$ (μb/sr) [b]	$-t$ (GeV/c)^2	$d\sigma/dt$ [μb/(GeV/c)^2] [b]
73.05	6.72±0.30±0.07	110.41	6.15±0.28	1.84	28.27±1.30
75.92	5.87±0.22±0.12	113.56	5.75±0.25	1.91	26.42±1.15
78.78	5.01±0.21±0.11	116.60	5.26±0.25	1.98	24.17±1.16
81.65	4.41±0.21±0.11	119.55	4.96±0.27	2.04	22.79±1.24
84.51	4.25±0.20±0.11	122.40	5.12±0.28	2.10	23.52±1.28
87.38	4.44±0.20±0.11	125.16	5.74±0.30	2.15	26.39±1.37
90.24	4.61±0.26±0.14	127.82	6.40±0.41	2.20	29.41±1.89
93.11	4.25±0.25±0.13	130.38	6.33±0.41	2.25	29.09±1.91
95.97	4.74±0.26±0.13	132.86	7.57±0.46	2.30	34.80±2.12
98.83	5.31±0.26±0.14	135.25	9.09±0.51	2.34	41.78±2.36
101.70	5.93±0.27±0.14	137.56	10.88±0.57	2.38	50.01±2.60
104.57	6.86±0.29±0.15	139.78	13.49±0.64	2.41	62.03±2.93

[a]Statistical and systematical uncertainties are given separately. The first quantity after the cross section value in this column is the statistical uncertainty and the second one is the systematical uncertainty.
[b]Uncertainties listed in this column are the total uncertanties, that is, the combination of statistical and systematical uncertanties.

The unpolarized differential cross sections at 792.7 MeV were doubly important to remeasure because the unpolarized cross sections supply the scale factor in an amplitude calculation and 800 MeV is the beam energy where most of the spin-observable data for *p-d* elastic scattering are concentrated. Although the differential cross sections over a large angular range were measured before[8] at 800 MeV, there were some internal inconsistencies in the paper that reported these data and, as explained in Sec. I, the laboratory cross sections tabulated in the paper could not give the reported center-of-mass values when the transformation was done properly. In fact, comparison with other data sets indicates that the center-of-mass values reported in the paper are the measured values. Apparently, these center-of-mass values were transformed to obtain the cross sections in the laboratory frame of reference. However, the Jacobian used in the transformation was the inverse of the correct Jacobian. Both the present data and the data of Winkelman *et al.*[8] are displayed in Figs. 5 and 6. It is clear that the center-of-mass values reported by Winkelman *et al.* are close to our measurement, although there is some disagreement at backward angles. This might be caused by the *p-p* quasielastic-scattering background which is lower in our case because of the liquid-deuterium target instead of the CD_2 target used by Winkelman *et al.*, and by a better determination of the true *p-d* elastic-scattering events (right or left scattering).

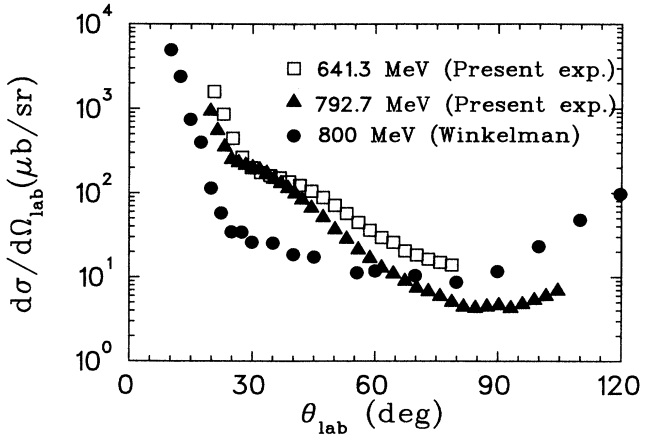

FIG. 5. Measured cross sections as a function of the proton-scattering angle in the laboratory frame of reference at 641.3 and 792.7 MeV for *p-d* elastic scattering. Previous 800 MeV cross section data from Ref. 8 are also displayed. Uncertainties are smaller than the plotting symbols.

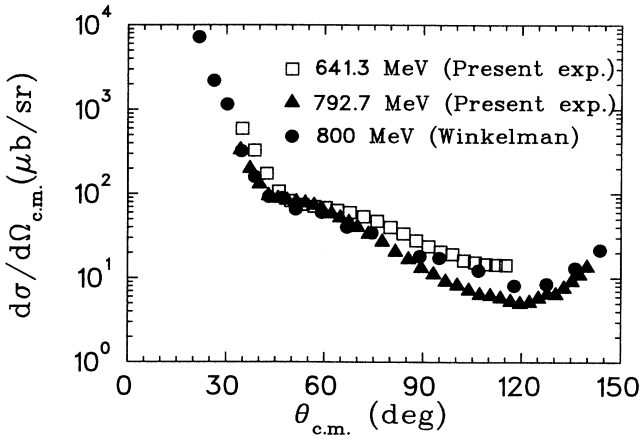

FIG. 6. Measured cross sections as a function of the proton-scattering angle in the c.m. frame of reference at 641.3 and 792.7 MeV for *p-d* elastic scattering. Previous 800 MeV cross section data from Ref. 8 are also displayed. Uncertainties are smaller than the plotting symbols.

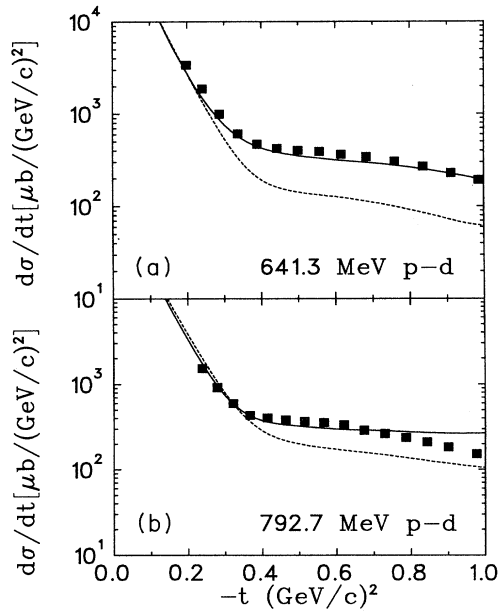

FIG. 7. The present measurements for *p-d* elastic scattering at (a) 641.3 MeV and (b) 792.7 MeV are plotted as $d\sigma/dt$ vs $-t$ and compared with theoretical calculations, RIA (broken lines), and relativistic multiple scattering (solid lines), as described in the text.

The unpolarized differential cross section data at 792.7 MeV beam energy were taken at eight different angular settings of the detector arms covering a combined angular range of 20° to 105° in the laboratory frame [35°–140° in the c.m. or $0.24 < -t < 2.41$ (GeV/c)^2] [Figs. 5,6,7(b), and Table II].

The uncertainties reported in Tables I and II include all the known contributions from systematical effects. For the cross sections in the laboratory frame of reference, the statistical and systematical uncertainties are given separately. The differential cross sections are listed as a function of angle (laboratory and c.m.) and four-momentum transfer ($-t$) in Tables I and II. The laboratory angles given in the tables are the midpoint values of the bins placed on the proton-scattering angles. The bin sizes are 30 mr at forward angles and 50 mr at other angles. Since the bin sizes are small, the weighted averages for the angles are not significantly different than the midpoint values of the bins. With the absolute cross section values reported here, an important component in amplitude calculations for the *p-d* elastic-scattering problem has been determined to significantly higher accuracy than that previously available.

Finally, experimental results are compared with theoretical calculations based on multiple-scattering models, expressing nucleon-nucleus scattering amplitudes in terms of *N-N* scattering amplitudes, and the nuclear wave functions.

In the case of *p-d* scattering, the total scattering amplitude is obtained in these models as a sum of single- and double-scattering terms, involving proton scattering off either one or both target nucleons. The single-scattering contributions can be unambiguously expressed in terms of the physical *N-N* scattering amplitude and the deuteron form factor. The double-scattering term, however, involves propagation of the projectile nucleon between the two scattering events, and therefore its evaluation requires additional information on the off-mass-shell behavior of the *N-N* amplitudes. One of the simplest assumptions is to represent relativistic *N-N* scattering amplitudes, both on- *and* off-mass-shell, as combinations of the usual five Fermi covariants, involving no momentum factors, and multiplied by invariant amplitudes depending only on the invariant energy and momentum transfers. This assumption is made in the relativistic-impulse approximation (RIA),[23] which has been successful in describing polarized proton scattering on heavy- and medium-weight nuclei.

Results obtained in the relativistic multiple-scattering model[24] using the RIA *N-N* off-mass-shell amplitudes are shown by broken line in Fig. 7. This calculations was done with *physical,* on-mass-shell amplitudes obtained from the recent solution SM89 to the *N-N* phase-shift analysis,[25] and with the deuteron wave function based on the Reid soft-core potential.[26] It is apparent that the RIA assumption does not reproduce correctly the differential cross section; comparison with spin observables[27] also shows poor agreement with the data.

The agreement with the experimental measurements can be significantly improved by allowing for an additional off-mass-shell dependence of the *N-N* scattering amplitude, which, physically, is expected to arise from the composite nature of nucleons,[28] and from derivative meson-nucleon couplings (some of them known, and some plausibly existing).[27] Specifically, the *N-N* scattering amplitude is then represented as

$$F(p',p)=\sum_{a=S,V,T,A,P}\sum_{I=0,1}\left[1+\xi_a^I\frac{\not p'-M}{2M}\right]K_a P_I A_a^I(p',p)\left[1+\xi_a^I\frac{\not p-M}{2M}\right], \tag{2}$$

where p and p' are the initial and final projectile nucleon momenta, A_a^I are invariant amplitudes (assumed to depend only on the energy and momentum transfer invariants), P_I are isospin operators projecting on states of isospin I in the exchange (t) channel, and the spin operators K_a, acting in the projectile- and target-nucleon spinor spaces, are the Fermi covariants: scalar (S), vector (V), tensor (T), axial (A), and pseudoscalar (P). On the mass shell, where the factors $(\not p-M)/2M$ vanish, Eq. (2) reduces to the standard representation of the *N-N* scatter-

ing amplitude. Off mass shell, and with vanishing parameters ξ, it reproduces the RIA form of the N-N scattering amplitude. In general, the dimensionless coefficients ξ generate an off-mass-shell dependence approximating that induced by derivative meson-nucleon couplings and by nucleon compositeness, in the sense of the low-energy derivative expansion.[27] They are regarded as phenomenological parameters to be adjusted, in reasonable limits, so as to fit the experimental observables. Such fits to the unpolarized cross section and all measured spin observables have been performed. At 800 MeV the fit, strongly constrained by the large number of spin observables available, gave parameter values $\xi_S^0=1.208-0.244i$, $\xi_V^0=-0.435+0.000i$, $\xi_T^0=-0.106-0.835i$, $\xi_A^0=-0.534-0.520i$, $\xi_P^0=0.790+1.155i$, $\xi_S^1=3.819-8.093i$, $\xi_V^1=-1.703-1.394i$, $\xi_T^1=1.060+2.474i$, $\xi_A^1=1.774+1.086i$, and $\xi_P^1=1.119+0.114i$. At 650 MeV, on the other hand, since only a few spin observables have been measured,[6,14] the results of the fit remain nonunique. A good fit to the measured observables has been obtained with only two nonvanishing complex parameters, $\xi_V^1=1.825+7.132i$ and $\xi_P^1=1.402-0.234i$, corresponding to the known ρ-N and π-N derivative couplings.[27] The cross sections calculated with these values of parameters are shown in Fig. 7 as solid curves.

In Fig. 7 the theoretical calculations are presented for four-momentum transfers up to $-t=1$ GeV$^2/c^2$. For larger four-momentum transfers the theories become unreliable because of uncertainties associated with off-mass-shell target nucleons, relativistic effects in the deuteron wave function, etc.[29]

As mentioned above, at 650 MeV the off-mass-shell parameters cannot be determined uniquely on the basis of the available measurements. For example, a fit equally good as that represented by the solid curve in Fig. 7(a) was obtained with the parameter set $\xi_V^1=2.757-5.490i$, $\xi_T^1=-0.829-0.067i$, and $\xi_P^1=0.117+0.311i$. However, these two parameter sets give quite different predictions for spin observables not known experimentally at the present time, in particular for the tensor asymmetry $C_{0NN,00}$. This implies that additional measurements of spin observables at 650 MeV would significantly constrain the choice of off-mass-shell parameters and thus provide valuable information about the off-mass-shell behavior of N-N amplitudes.

This work was supported in part by the U.S. DOE under Contract No. FG03-88ER40424.

*Present address: Los Alamos National Laboratory, Los Alamos, New Mexico 87545.

†Present address: Fermi National Accelerator Laboratory, P.O. Box 500, Batavia, Illinois 60510.

[1]D. V. Bugg, Annu. Rev. Nucl. Part. Sci. **35**, 295 (1985).

[2]J. C. Alder, W. Dolhoff, C. Lunke, C. F. Perdrisat, W. K. Roberts, P. Kitching, G. Moss, W. C. Olsen, and J. R. Priest, Phys. Rev. C **6**, 2010 (1972).

[3]N. E. Booth, C. Dolnick, R. J. Esterling, J. Parry, J. Scheid, and D. Sherden, Phys. Rev. D **4**, 1261 (1971).

[4]E. T. Boschitz, W. K. Roberts, J. S. Vincent, M. Blecher, K. Gotow, P. C. Gugelot, C. F. Perdrisat, L. W. Swenson, and J. R. Priest, Phys. Rev. C **6**, 457 (1972).

[5]M. G. Albrow, M. Borghini, B. Bosnjakovic, F. C. Erne, Y. Kimura, J. P. Lagnaux, J. C. Sens, and F. Udo, Phys. Lett. **35B**, 247 (1971).

[6]M. Moshi, Ph.D. thesis, University of California, Los Angeles, 1988.

[7]F. Irom, G. J. Igo, J. B. McClelland, C. A. Whitten, Jr., and M. Bleszynski, Phys. Rev. C **28**, 2380 (1983).

[8]E. Winkelmann, P. R. Bevington, M. W. McNaughton, H. B. Willard, F. H. Cverna, E. P. Chamberlin, and N. S. P. King, Phys. Rev. C **21**, 2535 (1980).

[9]A. Rahbar, B. Aas, E. Bleszynski, M. Bleszynski, K. Ganezer, G. J. Igo, F. Irom, B. E. Bonner, O. van Dyck, M. W. McNaughton, J. B. Roberts, C. Hollas, R. D. Ransome, and P. J. Riley, Phys. Lett. B **194**, 338 (1987).

[10]M. Haji-Saied, E. Bleszynski, M. Bleszynski, J. Carrol, G. J. Igo, T. Jaroszewicz, A. T. M. Wang, A. Sagle, J. B. McClelland, C. L. Morris, R. Klem, T. Joyce, Y. Makdishi, M. Marshak, B. Mossberg, E. A. Peterson, K. Ruddick, and J. Whittaker, Phys. Rev. C **36**, 2010 (1987).

[11]D. L. Adams, B. Aas, E. Bleszynski, M. Bleszynski, G. J. Igo, C. Newsom, Y. Ohashi, G. Pauletta, F. Sperisen, C. A. Whitten, Jr., H. Fujisawa, M. Gazzaly, S. G. Greene, K. Jones, J. B. McClelland, N. Tanaka, H. Hasai, K. Iwaani, S. Ishimoto, S. Isagawa, A. Masaike, A. Okihana, and S. Okumi, Nucl. Phys. **A480**, 530 (1988).

[12]V. Ghazikhanian, Ph.D. thesis, University of California, Los Angeles, 1988.

[13]A. N. Anderson, J. M. Cameron, D. A. Hutcheon, J. Källne, B. K. S. Koene, B. T. Murdoch, W. T. H. van Oers, and A. W. Stetz, Phys. Rev. Lett. **40**, 1553 (1978).

[14]Sun Tsu-hsun, B. E. Bonner, M. W. McNaughton, H. Ohnuma, O. B. van Dyck, G. S. Weston, B. Aas, E. Bleszynski, M. Bleszynski, G. J. Igo, D. J. Cremans, C. L. Hollas, K. H. McNaughton, P. J. Riley, R. F. Rodebaugh, S. Xu, and S. E. Turpin, Phys. Rev. C **31**, 515 (1985).

[15]E. Biegert, J. Carrol, W. Dragoset, Jr., R. Klem, J. Lesikar, M. L. Marshak, J. B. McClelland, T. Mulera, E. A. Peterson, J. B. Roberts, K. Ruddick, R. Talaga, and A. Wriekat, Phys. Rev. Lett. **41**, 1098 (1978).

[16]M. W. McNaughton, private communication.

[17]E. Gülmez *et al.*, Bull. Am. Phys. Soc. **34**, 1140 (1989).

[18]*Higher Energy Polarized Beams* (Ann Arbor, 1977), Proceedings of the Workshop, edited by A. D. Krisch and A. J. Salthouse, AIP Conf. Proc. No. 42 (AIP, New York, 1977), p. 142.

[19]E. Gülmez *et al.*, Bull. Am. Phys. Soc. **34**, 1798 (1989).

[20]E. Gülmez *et al.*, Nucl. Instrum. Methods A **297**, 7 (1990).

[21]E. Gülmez and C. A. Whitten, Jr., Nucl. Instrum. Methods A **297**, 17 (1990).

[22]D. Brown, Nucl. Instrum. Methods **117**, 561 (1974).

[23]R. J. Shepard, J. A. McNeil, and S. J. Wallace, Phys. Rev. Lett. **50**, 1443 (1983); B. C. Clark, S. Hama, L. R. Mercer, L. Ray, and B. D. Serot, *ibid.* **50**, 1644 (1983).

[24]E. Bleszynski, M. Bleszynski, and T. Jaroszewicz, in *Intersections Between Particle and Nuclear Physics* (Lake Louise, Canada), Proceedings of the Second Conference, edited by D. F. Geesaman, AIP Conf. No. 150 (AIP, New York, 1986), p. 1208.

[25]R. A. Arndt, L. D. Roper, R. A. Bryan, R. B. Clark, B. J.

VerWest, and P. Signell, Phys. Rev. D **28**, 97 (1983); amplitude analysis code SAID, 1989 version.
[26]W. Reid, Ann. Phys. (N.Y.) **192**, 233 (1982).
[27]M. Bleszynski and T. Jaroszewicz, UCLA report, 1990 (unpublished).
[28]E. Bleszynski, M. Bleszynski, and T. Jaroszewicz, Phys. Rev. Lett. **59**, 423 (1987).
[29]G. Alberi, M. Bleszynski, and T. Jaroszewicz, Ann. Phys. (N.Y.) **142**, 299 (1982).